NUMERICAL STUDY OF URM WALLS RETROFITTED WITH CABLE AND FRP

Y. ZHUGE

Senior Lecturer
School of Natural and Built Environments
University of South Australia
Mawson Lakes SA Australia

SUMMARY

The Australian love of "heritage" buildings (most of them are unreinforced masonry (URM)) means that greater attention is required to secure their performance under seismic loading in the future. This requirement highlights the need to improve the performance of URM by retrofitting and strengthening them to resist potential earthquake damages. In the past few years, several seismic retrofitting techniques for masonry structures have been developed and practiced. At the University of South Australia, two innovative retrofitting techniques using cable and fibre reinforced polymers (FRP) were developed to retrofit URM under in-plane shear. The experimental results showed that both the strength and ductility of tested specimens were significantly enhanced with these techniques. In this paper, an analytical model which is based on Distinct Element Method (DEM) has been developed to simulate the behaviour of URM walls before and after retrofitting by using these two retrofitting schemes. The analytical results have been compared with the available experimental testing data.

INTRODUCTION

Inherent advantages of masonry, including; aesthetics, heat and sound insulation, fire resistance and economical considerations, contribute to its continuing appeal. In Australia the majority of URM buildings have been constructed with little or no seismic requirement. This has resulted in a large inventory of buildings that possess an inability to dissipate energy through inelastic deformation in an earthquake event. Depending on the direction of the earthquake loads, two types of failure are commonly observed in load bearing URM walls subjected to seismic loads. These are in-plane failure characterized by a diagonal tensile crack pattern, and out-of-plane failure, where cracks are primarily along the mortar bed joints. The aim of seismic retrofitting is to upgrade the ultimate strength of the building by improving the structures ability to absorb inelastic deformation. This can be achieved by changing the structural system such that the energy is transferred along alternative load paths, or alternatively, increasing the ductility in the individual elements that make up the structural system.

There are many seismic retrofitting methods for URM walls, an extensive review and comparison of various retrofitting techniques is given in Chuang and Zhuge (2005). The application of FRP is one of the methods and has been increasingly used due to its high tensile strength, lightness and corrosion insensitivity. Using FRP for seismic retrofitting also has some more advantages like aesthetic, rapid application, durability, low cost of

installation, no loss of valuable space and can remain unchanging dynamic properties (mass) for structures. Another retrofitting method developed by the authors is to use cable (Chuang and Zhuge 2004). The cable retrofitting technique has similar advantages as FRP, but it costs less than using FRP. Unlike FRP, its mechanical behaviour is well understood. However, the testing results indicated that the cable retrofitting is less effective than FRP to improve the ultimate load carrying capacity.

In this paper, an analytical model which is based on Distinct Element Method (DEM) has been developed to simulate the behaviour of URM walls retrofitted by using these two different retrofitting techniques. In the distinct element method, a solid is represented as an assembly of discrete blocks. Joints are modelled as interface between distinct bodies. It is a dynamic process and specially designed to model the behaviour of discontinuities. By using DEM, the response of discontinuous media, such as unreinforced masonry, under both static and dynamic loading can be simulated.

The DEM model was successfully applied to simulate the response of URM shear wall panels in previous studies (Zhuge 1999; Zhuge and Hunt, 2003). In the current study, a new user defined FISH function has been developed to model the structural behaviour of cable and FRP. The debonding failure of FRP is modelled with a simplified bond slip model. The results between distinct element model and experiments are compared and discussed. The performance of cable and FRP retrofitting has been compared.

OUTLINE OF DISTINCT ELEMENT METHOD

The Distinct Element Method has been progressively developed over the past two decades. Cundall (1971) first introduced the Distinct Element Method to simulate progressive movements in blocky rock systems and the model has been implemented into a computer program UDEC since then.

In the DEM method, a solid is represented as an assembly of discrete blocks. Joints are modelled as interfaces between distinct bodies. The contact forces and displacements at the interfaces of a stressed assembly of blocks are found through a series of calculations, which trace the movements of the blocks (Itasca 2000). At all the contacts, either rigid or deformable blocks are connected by spring like joints with normal and shear stiffness k_n and k_s respectively. Similar to the Finite Element Method (FEM), the unknowns in the DEM are also the nodal displacements and rotations of the blocks. However, unlike FEM, DEM is a dynamic process and the unknowns are solved by the equations of motion. The speed of propagation depends on the physical properties of the discrete system. The solution scheme used by DEM is the explicit time marching scheme and it uses finite contact stiffness.

If the blocks are rigid, block displacements are calculated from out of balance moment and forces applied to the centre of gravity of each block. Resultant forces F include boundary forces applied to the edges of the block and gravity.

Newton's second law of motion is applied for each block:

$$\frac{\partial \dot{u}^{(t)}}{\partial t} = \frac{F^{(t)}}{m} \tag{1}$$

where $\dot{u}$ is the velocity, m is the mass, and t is the time.
Following the central difference integration scheme, Eq. (1) can be transformed into:

$$\dot{u}^{(t+\Delta t/2)} = \dot{u}^{(t-\Delta t/2)} + \frac{F^{(t)}}{m}\Delta t \tag{2}$$

For blocks in two dimensions where we assumed several forces acting on the block (including gravity load), the velocity (Eq. 2) can be re-arranged which includes angular velocity of block:

$$\begin{aligned}\dot{u}_i^{(t+\Delta t/2)} &= \dot{u}_i^{(t-\Delta t/2)} + (\frac{\sum F_i^{(t)}}{m} + g_i)\Delta t \\ \dot{\theta}^{(t+\Delta t/2)} &= \dot{\theta}^{(t-\Delta t/2)} + (\frac{\sum M^{(t)}}{I})\Delta t\end{aligned} \tag{3}$$

where $\dot{\theta}$ = angular velocity of block about centroid; I = moment of inertia of block; $\dot{u}_i$ = velocity components of block centroid; $\Sigma M^{(t)}$ = total moment acting on the block; $\Sigma F_i^{(t)}$ = total force acting on the block; and g_i = components of gravitational acceleration.

Assume velocities are stored at the half-time step point, the new velocities in Eq. (3) can be used to determine the new block location:

$$\begin{aligned}x_i^{(t+\Delta t)} &= x_i^{(t)} + \dot{u}_i^{(t+\Delta t/2)}\Delta t \\ \theta^{(t+\Delta t)} &= \theta^{(t)} + \dot{\theta}^{(t+\Delta t/2)}\Delta t\end{aligned} \tag{4}$$

where θ = rotation of block about centroid; and x_i = coordinates of block centroid.

The new position of the block induces new conditions at block boundaries and thus new contact forces. Resultant forces and moments are used to calculate linear and angular accelerations of each block. The calculation scheme summarised above by Eq. (1) to Eq. (4) is repeated until a satisfactory state of equilibrium or continuing failure is reached for each block. It should be noted that time has no real physical meaning if a static analysis was performed.

If the blocks are deformable, they will be internally discretised into finite difference triangular elements first before the equations of motion are formulated at each grid point.

The mortar joints are represented numerically as a contact surface formed between two block edges. The constitutive laws applied to the contacts are:

$$\Delta\sigma_n = k_n \Delta u_n \tag{5}$$

$$\Delta\tau_s = k_s \Delta u_s \tag{6}$$

where k_n and k_s are the normal and shear stiffness of the contact, $\Delta\sigma_n$ and $\Delta\tau_s$ are the effective normal and shear stress increments, and Δu_n and Δu_s are the normal and shear displacement increments.

Stresses calculated at grid points located along contacts are submitted to the selected failure criterion. For unreinforced masonry shear wall panels, the Coulomb friction is formulated:

$$\left|\tau_s\right| \le C + \sigma_n \tan\phi = \tau_{\max} \tag{7}$$

where C is the cohesion and ϕ is the friction angle.

There is also a limiting tensile strength f_t for the joint. If the tensile strength is exceeded, then $\sigma_n = 0$.

Modelling direct tensile splitting of brick is a more delicate subject. In order to simplify the problem, the brick unit material is modelled with Mohr-Coulomb failure criterion with tension cutoff. The shear flow rule is non-associated and the tensile flow rule is associated.

A detailed discussion of the model can be found in Zhuge and Hunt (2003).

SUMMARY OF EXPERIMENTAL PROCEDURES

Six full-scale clay brick masonry walls have been divided into two groups and each group was retrofitted with cable system and FRP respectively. The walls have been tested under combined compression and racking cyclic loads. Unreinforced masonry walls were also tested under the same loading condition for comparison purposes.

The proposed retrofitting systems aim to improve the performance of walls by increasing shear strength above their flexural strength and by increasing ductility and energy dissipation capability. All specimens were chosen with an aspect ratio of 1.0 to ensure that most of the unretrofitted walls would exhibit shear-induced damage. The dimensions of the wall were 940mm long x 940mm high x 110 wide (11 courses high and 4 bricks in each course). The wall was constructed on top of a concrete foundation beam to simulate a house footing.

The type of cable used for the experiment was Ronstan typical grade 316 stainless steel wire rope (19 single strands, Diameter 10mm, and breaking load of 71 kN) and ending for cable was seafast threaded swage terminals (RF1513M1010). The anchorage for the connection plate to the foundation beam was Ramset Chemset Anchor (M 16x190mm, design tensile and shear load 8.5 kN per anchor and Chemset 800 series).

The type of FRP used was Sika CarboDur S (width 30 mm, thickness 1.2mm and tensile strength of 2800 kN) and epoxy adhesive for bonding Sika CarboDur Strips was Sikadur-30.

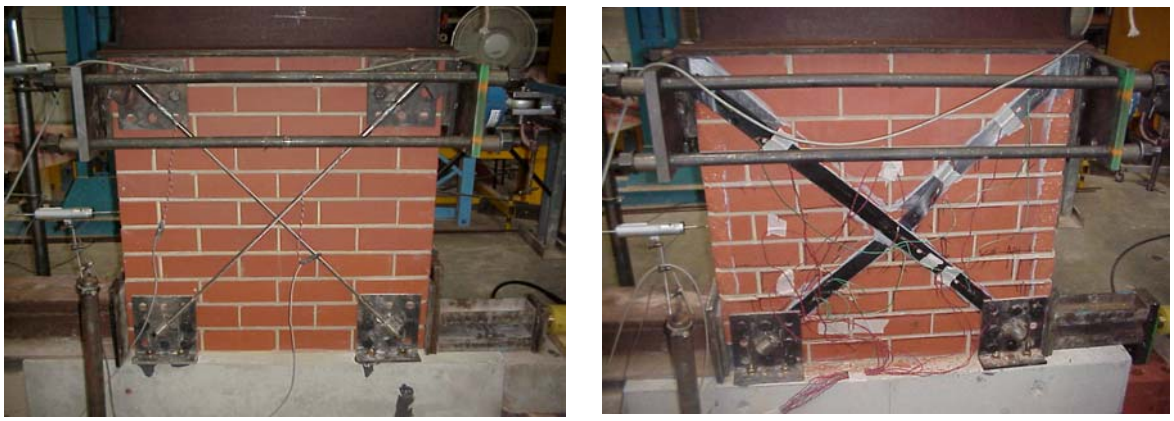

(a) Cable retrofit (b) FRP retrofit

Figure 1 – URM wall retrofitted with cable and FRP

Retrofit was accomplished by adding two 10mm diameter cables (wire ropes) or two 30 mm FRP on one side of the wall face, as shown in Figure 1. Ideally cables and FRP should be added on both sides of the wall to prevent an eccentric stiffness and strength distribution that may cause twisting of the retrofitted walls. The cable diameter was chosen to ensure that the wall would fail earlier than the cable. The anchor was designed for transferring the load from cable to foundation without failure before the cable is broken.

The tested walls were subjected to a constant vertical compressive stress σ_m = 0.2 MPa. To simulate earthquake loading, a series of horizontal displacement reversals of increasing amplitude were used on all the walls. The wall was cycled twice at each of the incrementally increasing displacement amplitude until failure. The specimens were well instrumented for displacement, rotation and strain measurements. Strain gauges were used to measure strains in cable and FRP.

NUMERICAL SIMULATION AND COMPARISON OF MASONRY WALLS RETROFITTED WITH CABLE AND FRP

Numerical simulation of URM walls retrofitted with cable or FRP is not an easy task. Masonry is not a simple material, the influence of mortar joints and bond as a plane of weakness is a significant feature. On the other hand, DEM is fully dynamic and it deals with pseudo-static problems by allowing the dynamic behaviour to reach equilibrium with notional time. It is specially designed to model the behaviour of discontinuities. Therefore, it is well suited for masonry structures. The DEM has been applied by the author to analyse the structural behaviour of URM (Zhuge 1999; Zhuge and Hunt 2003). The model was applied to simulate the response of an unreinforced masonry shear wall panel with and without an opening, where the experimental testing results are available. In general, good agreement is observed in the correlation (Zhuge and Hunt 2003).

Although DEM has been successfully applied to simulate URM walls under in-plane load, adding a cable is not straightforward. A special cable element was created in the model to simulate the axial behaviour of cable reinforcement which only carries uniaxial tensile force (Zhuge 2005). Different material properties were assigned to the unbonded section and anchorage section at the ends of the cable.

In the current paper, the model has been further developed to simulate FRP retrofitting. A special spring like element was created to simulate the bond (shear resistance) between the FRP and the host medium (masonry). In order to simplify the model, FRP was modelled as an equivalent one-dimensional element and only carries uniaxial tensile force (Figure 2). Axial displacements are computed based on integration of the laws of motion using the computed out-of-balance axial force and a mass lumped at each nodal point (Itasca 2000). The shear behaviour of the bond, during relative displacement between the FRP/bond interface and the bond/masonry interface, is described numerically by the bond shear stiffness and the maximum shear force that can be developed is limited by the cohesive strength of the bond. However, the properties related to the bond are more difficult to estimate. The bond stiffness may be determined from pullout test as for debonding failure modes, the stress state of the interface is similar to that in a pullout test (Chen and Teng 2003). As there are not enough pullout testing data available for masonry, the material properties of the adhesive adopted in this paper are from the pullout test of concrete and carbon FRP (Ueda and Dai 2005). The material properties of the cable and FRP are listed in Table 1.

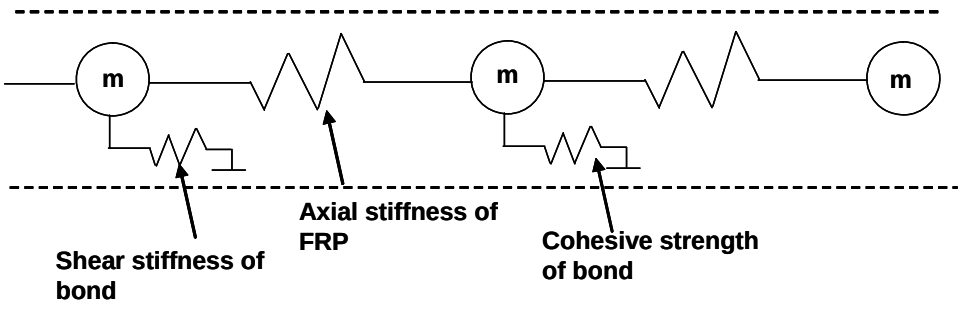

Figure 2 Conceptual representation of fully bonded FRP

Table 1 – Material Properties of Cable and FRP

				Unbonded section		Bonded section	
	E (MPa)	A (mm^2)	f_t (kN)	kbond (MPa)	sbond (MN/m)	kbond (N/m/m)	sbond (N/mm)
Cable	107500	78.5	71	1e-3	0	1e7	100
FRP	62000	36	2800	-	-	30e9*	180**

Where kbond is the bond shear stiffness and sbond is the cohesive strength of the bond.
*based on the shear stiffness of the adhesive layer, K_a = 1GPa/mm (Ueda and Dai 2005)
**based on the local bond strength τ_{max} = 6MPa (Ueda and Dai 2005).

k_n and k_s of the interfaces between the wall blocks are potentially important parameters in the numerical analyses of masonry walls using DEM . Unfortunately, there are very few testing data on stiffness properties for mortar joints are available. The only testing results the authors could find were the experiments conducted at the University of Delft, the Netherlands (Lourenco 1996). These testing results were used to validate the numerical model developed by the authors of masonry shear wall panels under in-plane lateral load (Zhuge & Hunt 2003). As the parametric studies indicated that the sensitivity of the results with respect to the estimation of joint material parameters was small, these values of k_n and k_s have been adopted again for the current model (Table 2).

Table 2. Summary of joint material properties

Tension	Shear			Normal stiffness	Shear stiffness
f_t (N/mm^2)	$\tan\phi$	$\tan\psi$	C (MPa)	k_n (N/mm^3)	k_s (N/mm^3)
0.25	0.75	0.0	0.375	82	36

COMPARISON BETWEEN EACH RETROFITTING SCHEME

The comparison between numerical and experimental load-displacement diagrams is shown in Figure 3. It can be seen from the figure that the experimental behaviour is well simulated by the numerical model for both retrofitting schemes. The collapse loads estimated by the numerical model was 40.7kN (cable) and 60.7kN (FRP) compared to the average experimental result of 43.4kN (cable) and 58.9kN (FRP) respectively. The sudden load drop around 17 kN (cable) and 37 kN (FRP) was due to major diagonal cracking occurring in the

wall which agreed well with experimental observations. The diagram also indicates the same initial stiffness of each wall until onsite of cracking and then the retrofitted walls behaved in a quite ductile manner. However, as the bond strength was assumed to behave as an elastic-perfectly plastic material, the descending branch could not be simulated by the current model. Nevertheless, the ultimate load capacity of the wall is well predicted by the model.

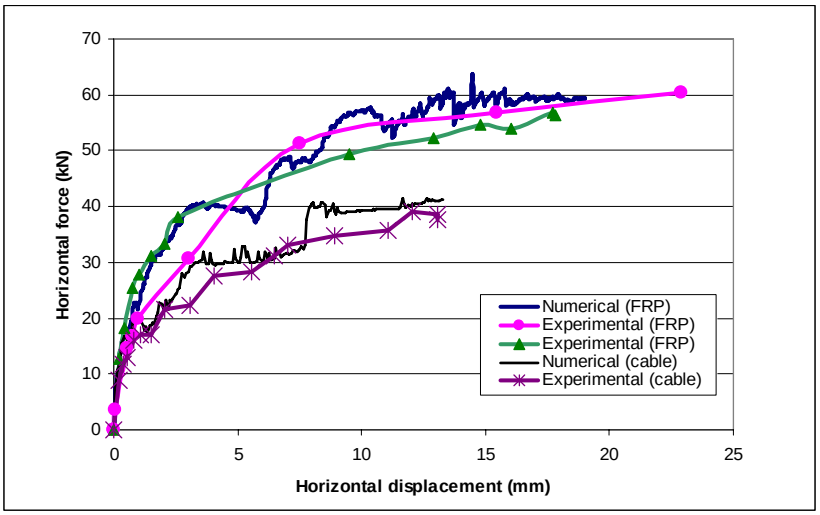

Figure 3 – Load-deflection Diagrams Comparison

During testing, all retrofitted walls exhibited superior behaviour when compared with those of URM walls. The ultimate load capacity of walls retrofitted with the cable and FRP increased around 2 and 3 times respectively. As indicated by Figure 4, similar results are predicted by the numerical model. Figure 4 also shows that when the wall was retrofitted with cable, it could not prevent the appearance of the crack (similar cracking loads were predicted for walls with and without cable, indicated by a sudden load drop around 20 kN) as anchorage was only provided at each end of the cable. However, for walls retrofitted with FRP, a higher cracking load was predicated and this was due to the full bonding between masonry and FRP. For URM wall, major cracks were developed along the diagonal direction, the wall failed due to compressive crushing at the supports and rotated as rigid bodies. For wall retrofitted with cable and FRP, they could prevent the development of the main diagonal cracks and allow the cracks to spread more evenly over the entire wall. The wall then could continue to carry higher load. This also agrees with the experimental results.

The force carried by FRP and cable and the force carried by the whole retrofitted wall are also compared (Figure 5). The experimental results indicated that FRP carried around 50% of the force acted on the whole wall even at the early loading stage whereas for cable retrofitted walls, this only happened after the major diagonal crack formed. The numerical model showed a good agreement with testing results of the forces carried by FRP until the debonding failure occurred (Figure 5a). A higher ultimate force was predicated by the model followed by the sudden drop of the load. However, it should be noted that due to the location of strain gages, the FRP forces obtained from the testing were not the maximum axial force. Past research has indicated that the axial forces in FRP were not uniformly distributed at the ultimate stage (Chen and Teng 2003) and this was proved by the model as shown in Figure 6. The numerical predication of the forces carried by cable is not as good as for FRP. As indicated in Figure 5b, cable carried around 80% of the force when the wall reached its ultimate strength which was not in agreement with testing result. Due to the limitation of the software and DEM, it is very difficult to model a steel plate attached to URM walls.

Therefore, the equivalent bonding stiffness and strength were assigned to the cable and wall connection whereas for FRP, the bonding stiffness and strength were obtained from a large number of testing database. Nevertheless, the ultimate load capacity of the wall is well predicted by the model for both retrofitting schemes.

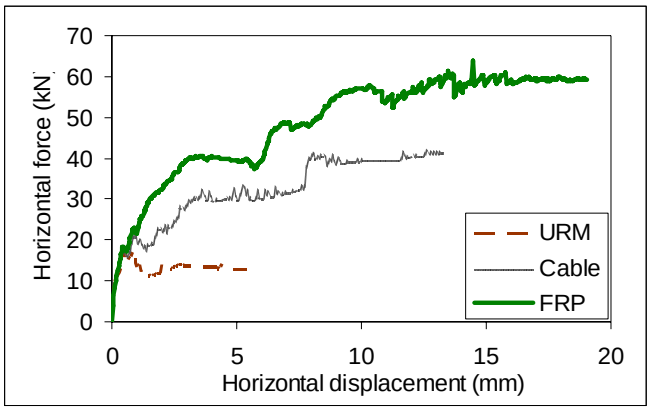

Figure 4 - Simulated behaviour of the walls with two retrofitting schemes

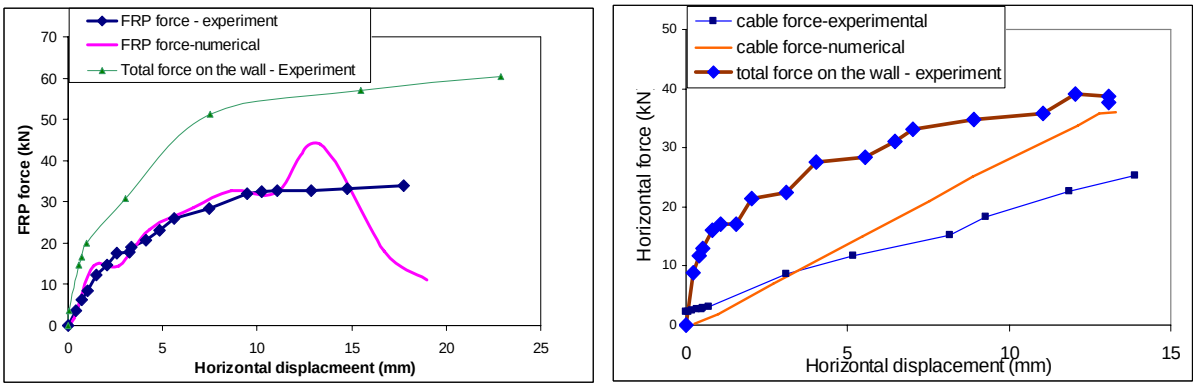

(a) FRP retrofitted wall (b) Cable retrofitted wall

Figure 5 Comparison of forces carried by FRP, cable and the wall

The above discussion of the wall behaviour can be demonstrated by the minimum principal stresses distribution shown in Figure 7. For URM wall (Figure 7(a)), when the diagonal cracks are fully open, two distinct struts are formed, one at each side of the diagonal crack. The concentration of the large compressive stress at the supports leads to the collapse of the wall. However, for cable retrofitted wall (Figure 7(b)), the full opening of the diagonal cracks was prevented by the existence of cable; two distinct struts are not formed. The large compressive stresses were mainly carried by the anchorage through the two steel plates at the end of the cable. However, for FRP retrofitted wall (Figure 7(c)) under the same displacement, several small struts were formed and oriented parallel to the diagonal line as FRP prevented the formation of the diagonal crack at this loading stage. A more continuous stress distribution was observed.

CONCLUSIONS

Numerical modelling of masonry is not an easy task due the influence of mortar joints as a plane of weakness. In the past few years, an alternative and simple way of modelling masonry which uses the Distinct Element Method has been developed by the author and validated by the testing results. In this paper, the model is further developed to investigate the behaviour of unreinforced masonry walls retrofitted with two different schemes.

The model is validated by comparing the results with those obtained from the experiments, which include the force-displacement diagram, ultimate load capacity and the failure pattern of the wall with and without retrofitting. The debonding failure of FRP was well modelled. The material properties of the bond-slip model were obtained from a large experimental data base for FRP bonded to concrete as no such data available for masonry. The results predicted for cable retrofitting were not as good as for FRP as it is very difficult to model the anchorage through the steel plate using DEM. The performance of two retrofitting schemes has been compared. It proves that FRP retrofitting is more effective than cable and cable retrofitting could not prevent the formation of cracking. However, cable retrofitting could increase the ultimate strength of the URM wall twice and cost less. The analysis has confirmed the experimental results that using either FRP or cable to retrofit low-rise masonry walls is an effective technique to significantly increase the in-plane strength, ductility, and energy dissipation capacity. The model developed in this paper also promised a further study of the bond-slip model for FRP bonded to masonry walls.

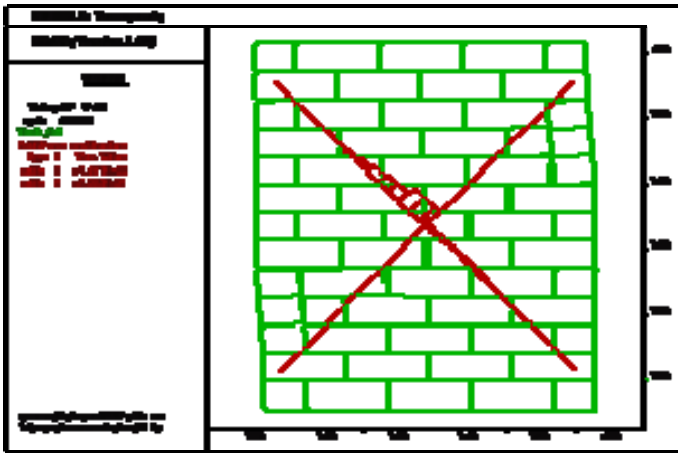

Figure 6 Axial forces carried by FRP

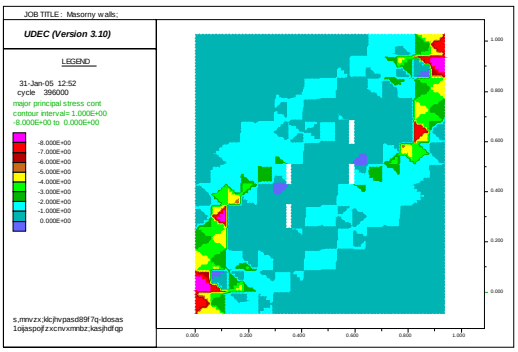

(a) URM wall

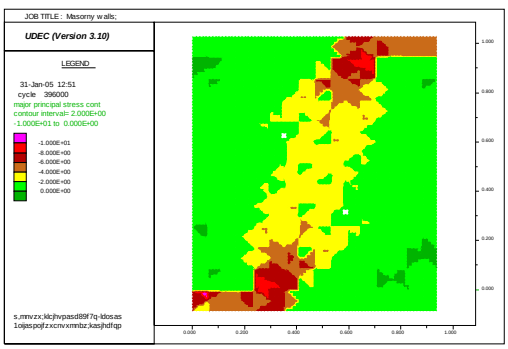

(b) Retrofitted wall - cable

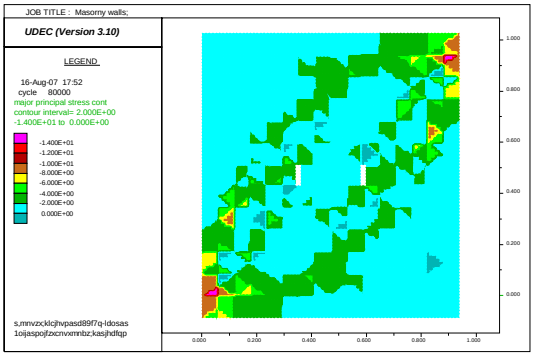

(c) Retrofitted wall – FRP

Figure 7 - Principal Stress Distributions from DEM

REFERENCES

Chen, JF and Teng, JG, "Shear capacity of FRP-strengthened RC beams: FRP debonding", Const. & Building Mat. 17, 2003, 27-41.

Chuang, S. and Zhuge, Y., "Seismic retrofitting of unreinforced masonry walls by FRP strips and cable system", *18th Australasian Conference on the Mechanics of Structures and Materials*, Perth, Australia. Dec., 2004, pp. 49-54.

Chuang, Y. and Zhuge, Y., "Seismic Retrofitting of unreinforced Masonry – A Literature Review". *Australian Journal of Structural Engineering*, Vol.6, No 1, 2005, pp. 25-36.

Cundall, P. A. A Computer Model for Simulating Progressive Large Scale Movements in Blocky Rock Systems. *Proceedings of the Sym. of the International Society for Rock mechanics*, Nancy, Francs, Vol. 1, II-8, 1971, pp. 11-18.

ITASCA Consulting Group. Universal Distinct Element Code. ITASCA consulting Group, Inc., Minneapolis, Minnesota, USA, 2000.

Lourenco, P. B. Computational Strategies for Masonry Structures. PhD Thesis, Delft University of Technology, The Netherlands, 1996.

Ueda, T. and Dai, J.G., "New shear bond model for FRP-concrete interface – from modelling to application", *FRP Composites in Civil Engineering*, London, 2005, pp. 69-81.

Zhuge, Y. Distinct Element Modelling of Unreinforced Masonry Walls. *Proc. of the 7th East Asia-Pacific Conference of Structural Eng. and Construction*, Kochi, Japan, 1999, pp. 411-416.

Zhuge, Y. and Hunt, S. Numerical Simulation of Masonry Shear Panels with Distinct Element Approach. *Structural Eng. And Mechanics – an International Journal*, Vol. 15, No4, 2003, pp. 477–493.